



Contents lists available at [SciVerse ScienceDirect](http://www.sciencedirect.com)

# Bioorganic & Medicinal Chemistry Letters

journal homepage: [www.elsevier.com/locate/bmcl](http://www.elsevier.com/locate/bmcl)



## Discovery and optimization of potent and selective imidazopyridine and imidazopyridazine mTOR inhibitors

Emily A. Peterson<sup>a,\*</sup>, Alessandro A. Boezio<sup>a,\*</sup>, Paul S. Andrews<sup>b</sup>, Christiane M. Boezio<sup>a</sup>, Tammy L. Bush<sup>d</sup>, Alan C. Cheng<sup>e</sup>, Deborah Choquette<sup>a</sup>, James R. Coats<sup>a</sup>, Adria E. Colletti<sup>c</sup>, Katrina W. Copeland<sup>a</sup>, Michelle DuPont<sup>d</sup>, Russell Graceffa<sup>a</sup>, Barbara Grubinska<sup>d</sup>, Joseph L. Kim<sup>f</sup>, Richard T. Lewis<sup>a</sup>, Jingzhou Liu<sup>c</sup>, Erin L. Mullady<sup>b</sup>, Michele H. Potashman<sup>a</sup>, Karina Romero<sup>a</sup>, Paul L. Shaffer<sup>f</sup>, Mary K. Stanton<sup>g</sup>, John C. Stellwagen<sup>a</sup>, Yohannes Teffera<sup>e</sup>, Shuyan Yi<sup>a</sup>, Ti Cai<sup>d</sup>, Daniel S. La<sup>a</sup>

<sup>a</sup> Medicinal Chemistry, Amgen Inc., 360 Binney St., Cambridge, MA 02142, USA

<sup>b</sup> Lead Discovery, Amgen Inc., 360 Binney St., Cambridge, MA 02142, USA

<sup>c</sup> Pharmacokinetics and Drug Metabolism, Amgen Inc., 360 Binney St., Cambridge, MA 02142, USA

<sup>d</sup> Oncology Research, Amgen Inc., 360 Binney St., Cambridge, MA 02142, USA

<sup>e</sup> Molecular Structure, Amgen Inc., 1120 Veterans Blvd., South San Francisco, CA 94080, USA

<sup>f</sup> Molecular Structure, Amgen Inc., 360 Binney St., Cambridge, MA 02142, USA

<sup>g</sup> Pharmaceuticals R&D, Amgen Inc., 360 Binney St., Cambridge, MA 02142, USA

### ARTICLE INFO

#### Article history:

Received 15 May 2012

Revised 6 June 2012

Accepted 11 June 2012

Available online 16 June 2012

#### Keywords:

mTOR

Kinase inhibitor

Oncology

Imidazopyridine

Imidazopyridazine

### ABSTRACT

mTOR is a critical regulator of cellular signaling downstream of multiple growth factors. The mTOR/PI3K/AKT pathway is frequently mutated in human cancers and is thus an important oncology target. Herein we report the evolution of our program to discover ATP-competitive mTOR inhibitors that demonstrate improved pharmacokinetic properties and selectivity compared to our previous leads. Through targeted SAR and structure-guided design, new imidazopyridine and imidazopyridazine scaffolds were identified that demonstrated superior inhibition of mTOR in cellular assays, selectivity over the closely related PIKK family and improved in vivo clearance over our previously reported benzimidazole series.

© 2012 Published by Elsevier Ltd.

The mammalian target of rapamycin (mTOR) kinase has been identified as a critical signaling node in the promotion of cancer cell growth and survival.<sup>1</sup> The mTOR pathway senses the cellular availability of nutrients and energy, serves as a downstream regulator of growth factor signaling, and is ultimately responsible for mediating cell functions such as apoptosis, autophagy, translation, cell cycle regulation and cytoskeleton reorganization. mTOR functions through two distinct multi-protein complexes, each defined by the interaction of mTOR with either Raptor (regulatory-associated protein of mTOR) as in the case of mTORC1 or Rictor (rapamycin-insensitive companion of mTOR) as in the case with mTORC2. mTOR complex 1 (mTORC1) acts as an integral participant in translation and cell growth by phosphorylation of substrates 4EBP1 and S6K, whereas mTOR complex 2 (mTORC2) acts to fully activate signaling

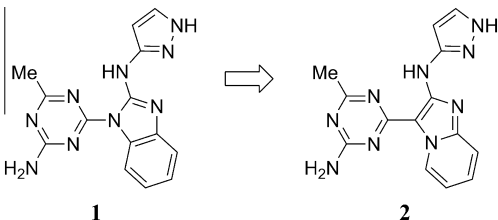
through AKT by phosphorylation of S473. Both complexes play critical roles in the PI3K/AKT cascade, a pathway wherein mutations within its signaling components are frequently present in cancer cells.

As an oncology target, mTOR has been validated in humans by the clinical use of rapamycin analogues Torisel® (Temsirolimus)<sup>2</sup> and Afinitor® (Everolimus),<sup>3</sup> both allosteric inhibitors of mTORC1. While these inhibitors have shown promising results in a limited number of cancers, it has been reported that selective inhibition of mTORC1 by rapamycin can increase AKT signaling through elimination of the negative feedback mechanism with IRS1.<sup>4</sup> The goal of our program was to develop an ATP-competitive mTOR inhibitor that would block the activity of both mTORC1 and mTORC2 and demonstrate selectivity over kinases within the highly homologous PIKK family, especially PI3K $\alpha$ . The rationale for this decision was the expectation that a selective inhibitor of mTOR could demonstrate increased tolerability compared to a dual mTOR/PI3K $\alpha$  inhibitor due to the effects of PI3K $\alpha$  inhibition on glucose homeostasis.<sup>5</sup> A significant amount of research aimed at developing

\* Corresponding authors. Tel.: +1 617 444 5027; fax: +1 617 621 3907 (E.A.P.); tel.: +1 617 444 5104; fax: +1 617 621 3908 (A.A.B.).

E-mail addresses: [epeterso@amgen.com](mailto:epeterso@amgen.com) (E.A. Peterson), [aboenzio@amgen.com](mailto:aboenzio@amgen.com) (A.A. Boezio).

**Table 1**  
Comparison of benzimidazole and imidazopyridine



Compound	1	2
<i>Biochemical and cellular assays (nM)</i>		
mTOR <sup>a</sup>	23	12
PI3K $\alpha$ <sup>b</sup>	798 (35X)	590 (49X)
PI3K $\beta$ <sup>b</sup>	875 (38X)	1130 (94X)
p4EBP1 <sup>c</sup>	391	162
pAKT <sup>d</sup>	55	19
pS6 <sup>e</sup>	166	69
<i>Solubility (<math>\mu\text{g/mL}</math>)<sup>f</sup></i>		
PBS	8.4	6.3
SIF	8.4	27
0.01 N HCl	3.7	>200
<i>Permeability (Human LLC-PK1 cells, <math>\mu\text{m/s}</math>)</i>		
P APP A2B	20.3	13.8
P APP B2A	35.4	33.7
Efflux Ratio	1.7	2.4
<i>IV Rat PK (dose = 1.0 mg/kg)<sup>g</sup></i>		
Cl (L/h/kg)	1.9	1.8
V <sub>ss</sub> (L/kg)	1.1	1.1
T <sub>1/2</sub> (h)	0.72	0.45
PO (%F) <sup>h</sup>	6	24
<i>Selected calculated properties</i>		
cLogP <sup>i</sup>	1.84	1.78
PSA ( $\text{\AA}^2$ )	123.2	122.7
Global pKa <sup>j</sup>	2.39	2.53

<sup>a</sup>  $n \geq 2$ , inhibition of kinase activity (Lantha-Screen).

<sup>b</sup>  $n \geq 2$ , inhibition of kinase activity (Alpha-screen).

<sup>c</sup>  $n \geq 2$ , cell assay measuring p4EBP1 in U87 cells.

<sup>d</sup>  $n \geq 2$ , cell assay measuring pAKT (S473) in U87 cells.

<sup>e</sup>  $n \geq 2$ , cell assay measuring phosphorylation of mTOR substrate S6 (S240/244) in U87MG cells.

<sup>f</sup> Symyx solubility system.

<sup>g</sup> Formulation = 100% DMSO.

<sup>h</sup> 1%Tween 80, 2%HPMC, 97% H<sub>2</sub>O, pH=2.2 (methanesulfonic acid).

<sup>i</sup> Daylight method.

<sup>j</sup> ACD method.

ATP-competitive mTOR inhibitors has recently been reported,<sup>6</sup> including our own discovery of benzimidazole triazines, which showed selectivity over related PIK family members as well as across the broader kinome.<sup>7</sup> While benzimidazole **1** provided important proof of concept, it showed low, nonlinear exposure when dosed orally due to poor solubility (Table 1).<sup>8</sup> Herein we report our efforts to address the undesirable physicochemical properties of this series while seeking enhanced potency and selectivity as well as improved ADME properties.

We attributed the poor bioavailability of **1** to poor aqueous solubility, since permeability was high and there was minimal efflux observed. There are several strategies one might employ to improve the aqueous solubility such as lowering cLogP, altering the pK<sub>a</sub>, disrupting molecular planarity by disrupting aromaticity or introducing unsaturation.<sup>9</sup> Our attempts to incorporate these strategies were met with varying success. The cLogP for **1** is 1.84, a value low enough that further reduction by the incorporation of additional heteroatoms would increase the already high PSA and the potential for efflux. Alternatively, introducing saturation into any of the three rings led to significant loss of potency or compound instability. A more subtle approach to disrupting molecular planarity would be to move one of the benzimidazole nitrogens into a bridgehead position. It has been previously hypothesized that a bridgehead nitrogen in a fused aromatic ring system can

introduce an infinitesimal twist in the framework that is enough to perturb molecular packing enough to improve solubility.<sup>9b</sup> To test this hypothesis, the benzimidazole nitrogen was transposed to provide imidazopyridine **2** (Table 1). This change maintained the broader planarity between the triazine hinge-binder and the imidazopyridine ring, which was previously shown to be essential for maintaining good potency. The calculated global pK<sub>a</sub>, and the cLogP were also minimally affected by this change. The pK<sub>a</sub> was increased for the imidazopyridine relative to the benzimidazole scaffold and the cLogP value was decreased by this subtle structural change, both factors known to improve aqueous solubility. This small structural mutation led to a significant improvement with regard to solubility and bioavailability when compared to benzimidazole **1**, as evidenced by the improved solubility measured in SIF and HCl solutions. This critical advancement represented a major turning point in the program, as it addressed one of the key PK flaws of the benzimidazole series reported earlier. The selectivity over related PI3K kinases and the broader kinome was also maintained, with **2** showing exquisite selectivity over the 402 kinases tested, attenuating concerns for potential confounding pharmacology in an in vivo setting.<sup>10</sup>

The improvement in bioavailability provided the opportunity to test **2** in vivo to establish target coverage and tumor growth inhibition using an orally administered compound.<sup>11</sup> To confirm that **2** inhibits mTOR activity in vivo, mice were administered a single dose of vehicle or **2** at 10, 30 and 100 mg/kg. As shown in Figure 1A, administration of **2** for 6 h resulted in significant dose-dependent inhibition of pAKT (at both S473 and T308 sites) and pS6<sup>12</sup> in HGF-stimulated mouse liver tissue compared to vehicle-controls ( $p \leq 0.0368$ ).<sup>13</sup> The downstream target of PI3K $\alpha$  (through PDK1), pAKT (T308), was inhibited to a lesser degree with the higher 30 and 100 mg/kg doses, demonstrating desired target selectivity in vivo. Furthermore, the drug concentrations measured in plasma reflected the degree of mTOR inhibition (Fig. 1A). After correcting for protein binding, the measured in vivo IC<sub>50</sub> for pAKT (S473) and pS6 were 53 and 71 nM, respectively, which corresponded well with the values measured in the in vitro cellular assays (Table 1).

A subsequent time-course mouse liver pharmacodynamic study was conducted with 100 mg/kg at 3, 6, 8 and 24 h to understand duration of target coverage (data not shown). Oral administration of **2** resulted in statistically significant inhibition of pAKT (at both S473 and T308 sites) and pS6 greater than 8 hours with recovery by 24 h. In anticipation of a long-term efficacy study, we first evaluated two high doses, 60 and 100 mg/kg ( $n = 5$  per group), in a 7-day tolerability study (data not shown). After 3 days, mice dosed with 100 mg/kg daily (QD) resulted in body weight loss (average >20%) and were removed from the study. In contrast, 60 mg/kg dosed QD for 7 days was well tolerated, suggesting this dosage could be used as the maximum starting dose for the xenograft study.

To compare the inhibition of mTOR activity (as measured by the degree and duration of pAKT and pS6 inhibition) with suppression of tumor growth in vivo, a tumor xenograft assay was performed. Mice bearing established U87-MG tumors were orally administered vehicle alone or **2** at 10, 30 or 60 mg/kg QD or 30 mg/kg twice daily (BID) continuously throughout the study. As shown in Figure 1B, continuous administration of **2** resulted in significant tumor growth inhibition (TGI) that was dose-dependent compared to vehicle-controls [60 mg/kg (82%) QD or 30 mg/kg (84%) BID;  $p \leq 0.0001$ ]. Encouraged by the robust in vivo response to treatment with **2**, the focus of our efforts turned to further improvement of this promising scaffold. Consideration of the target coverage required to achieve significant TGI, as well as the potency and pharmacokinetic properties of **2**, prompted further investigation into how the potency, in vivo clearance properties and selectivity of **2** could be improved to provide an mTOR inhibitor with qualities more suitable for drug development.

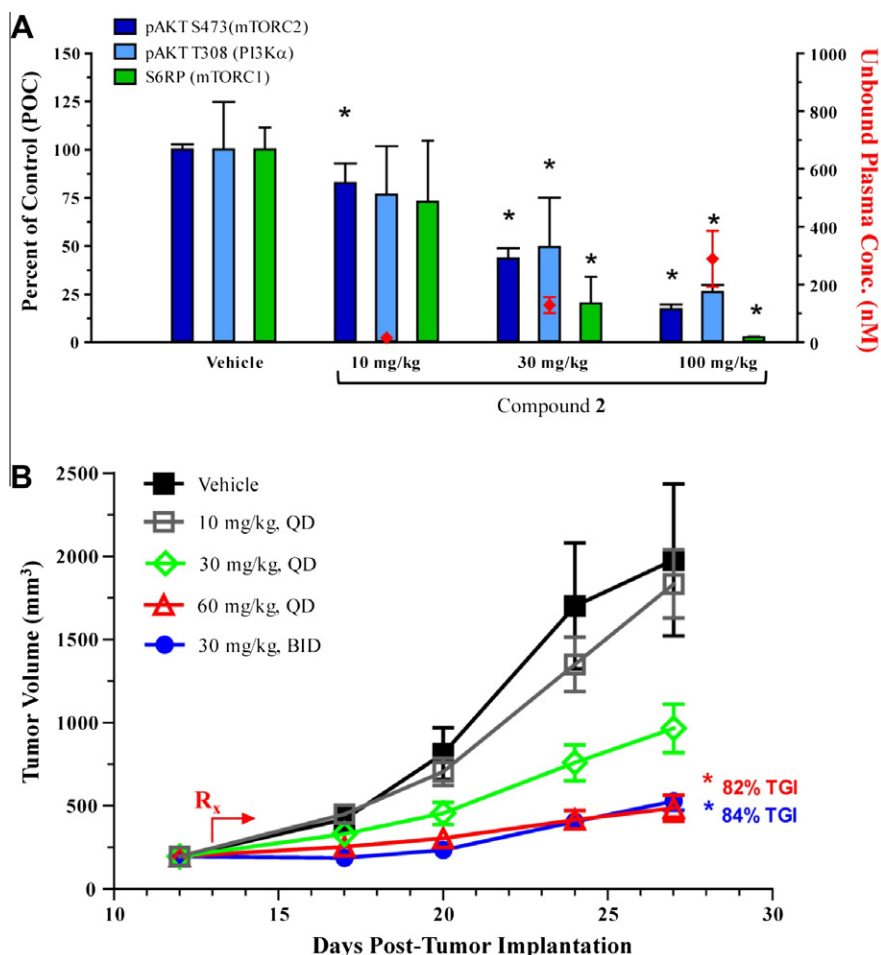
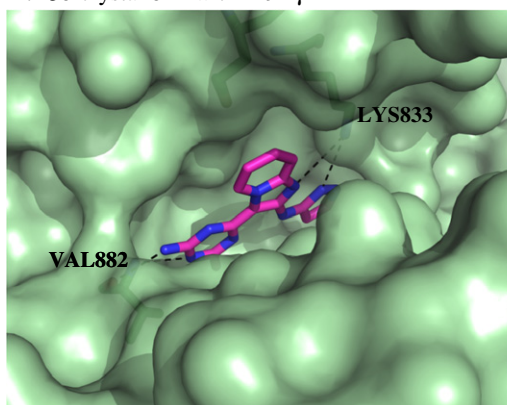


**Figure 1.** Compound **2** inhibits phosphorylation of mTOR substrates in mouse liver tissue and the growth of U87-MG tumor xenografts. (A) Bar graph representing the pharmacodynamic-pharmacokinetic assay measuring changes in HGF-induced phosphorylation of pAKT and pS6RP after a single oral dose of vehicle alone (50% PEG400, 1% Pluronic F68, pH 2.2 with MSA) or **2** at 10, 30 or 100 mg/kg ( $n = 3$  per dose) at 6 h. (B) Mice bearing established U87-MG tumors were orally administered vehicle (■) or **2** at 10 (□), 30 (◇), 60 mg/kg (△) QD or 30 mg/kg (●) BID for 2 weeks. Tumor volumes (mm<sup>3</sup>) are represented as mean  $\pm$  SE ( $n = 10$ ). Asterisk (\*) indicates statistical significant inhibition compared to vehicle-control determined by Factorial ANOVA (A,  $p < 0.0368$ ) or repeated measures analysis of variance (RMANOVA) (B,  $p < 0.0001$ ) followed by Dunnett's test for multiple comparisons.

In an attempt to decrease the amount of drug required to achieve robust tumor growth inhibition, efforts were first focused on improving the potency of **2**. An X-ray co-crystal structure of **2**<sup>14</sup> with structurally related kinase PI3K $\gamma$  was obtained in order to understand how **2** was interacting with the kinase active site. (Fig. 2A).<sup>15</sup> The primary hydrogen bonding interactions, which

are likely conserved within the mTOR active site, are between the triazine amine and the kinase hinge residue VAL882 as well as the interaction of the catalytic LYS833 with the pyrazole and the imidazopyridine core. The imidazopyridine core occupies the space where the ribose sugar moiety of ATP would reside. Extensive SAR had already been performed to optimize the methyl group

A. Co-crystal of **2** with PI3K $\gamma$



B. Inhibitor **12** in mTOR homology model

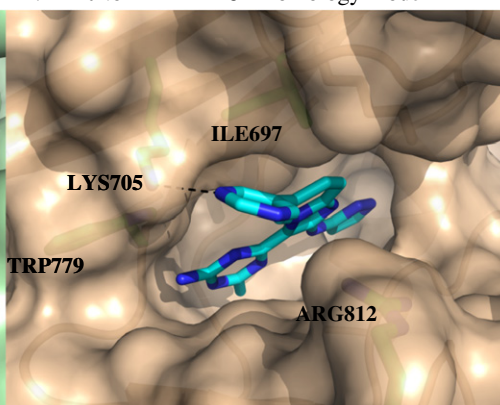


**Figure 2.** Structural design elements. (A) Co-crystal of **2** with PI3K $\gamma$ . (B) Inhibitor **12** in mTOR homology model.

**Table 2**  
Exploration of the ribose pocket

Compd	R	IC <sub>50</sub> (nM)			
		mTOR	PI3K $\alpha$	4EBP1	pAKT
<b>2</b>	H	12	590 (49X)	162	19
<b>3</b>		15	648 (43X)	67	64
<b>4</b>		27	654 (24X)	912	73
<b>5</b>		6	306 (55X)	326	26
<b>6</b>		3	119 (36X)	101	12
<b>7</b>		3	120 (48X)	41	10
<b>8</b>		21	393 (19X)	652	54
<b>9</b>		2	73 (47X)	49	13
<b>10</b>		39	268 (7X)	510	138
<b>11</b>		4	239 (64X)	222	23
<b>12</b>		2	85 (37X)	93	5
<b>13</b>		3	68 (24X)	57	6
<b>14</b>		10	96 (9X)	115	29
<b>15</b>		5	463 (98X)	276	23
<b>16</b>		2	144 (63X)	58	8
<b>17</b>		3	177 (71X)	72	7

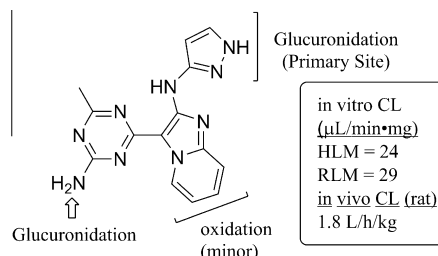


**Figure 3.** Metabolism of **2** in rats.

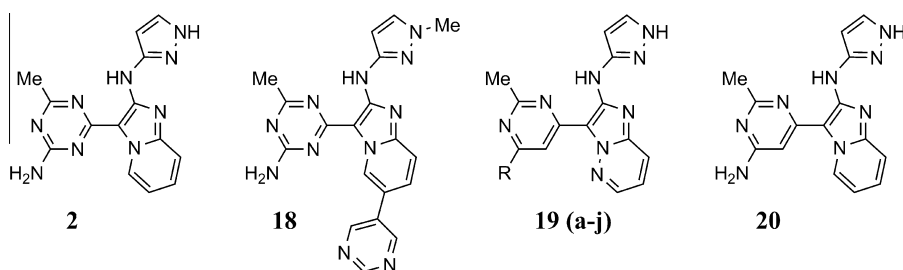
on the triazine hinge-binder, which was optimal for provision of broader kinase selectivity. In addition, the pyrazole affinity pocket group was uniquely effective at providing potency and selectivity over PI3K $\alpha$ .<sup>7</sup> Further examination of the PI3K $\gamma$  co-crystal structure with **2** revealed two areas where additional SAR might be developed to improve the potency and selectivity for mTOR (Fig. 2A). The remaining positions that had not been investigated were the substitution of the amine hinge binder and extension into the ribose pocket from either the 6 or 7-position of the imidazopyridine ring. Interestingly, both positions also suggested potential for improving selectivity due to residue differences between the PI3K family versus mTOR (Fig. 2B, vide infra).<sup>16</sup>

The first area that was explored was substitution of the imidazopyridine ring (Table 2). To preserve the co-planarity of the triazine and imidazopyridine rings considered essential for potency, substitution of the 5-position was not investigated, since any substitution would likely disrupt planarity. Further examination of the structure depicted in Figure 2A revealed that the 6 and 7-positions had the most space available and coincidentally were the most accessible from a synthetic standpoint. Substitution at the 7-position was tested and did not result in an improvement in potency over the parent **2**, whereas introduction of aromatic substituents at the 6-position provided an improvement in potency (Table 2). The data in Table 2 summarize the SAR findings from substitution of the 6-position. A variety of substituents were tested at this position including aliphatic, alkoxy, amide, alkenyl, alkynyl, aromatic and heteroaryl with varying substitutions. In general, cellular potency was improved with heteroaryl substituents, giving IC<sub>50</sub>s < 100 nM for inhibition of the p4EBP1 assay.

As predicted by analysis of the mTOR homology model shown with inhibitor **12** in Figure 2B, aryl groups containing a nitrogen at the meta-position gave the best boost in potency, presumably due to a favorable interaction with LYS705. The proximity of residues LYS705 and ARG 812 to the two meta-positions of the pyrimidine also rationalized why substituents at the 3-position of the aryl ring did not lead to a potency improvement (**4**, **11**, **14**). Introduction of a methyl group *ortho* to the ring attachment also provided an increase in mTOR cellular potency, but only in the presence of the meta-nitrogen group (Table 2, **6**, vs **7**, vs **8**). This combination resulted in a mTOR p4EBP1 cellular potency of 41 nM.<sup>17</sup> This additional potency improvement could be a result of the methyl group enforcing the twisted conformation shown in Figure 2B, locking the substituent in a favorable conformation for interaction with the adjacent LYS705 and avoiding a potential steric clash with adjacent ILE697. Five-membered heterocycles were also effective at significantly increasing the cellular potency (Table 2, **15**–**17**). The potency improvement observed by adding an aromatic substituent at the 6-position was encouraging, but was tempered by the observation that the binding efficiency (BE) was diminished as was selectivity over PI3K $\alpha$ . Furthermore, pharmacokinetics remained a major hurdle for this series, in particular the high in vivo clearance,

**Table 3**

Exploring the imidazopyridazine core and substitution of the linker-binder pyrimidine



Compd	R	IC <sub>50</sub> (nM)			Rat PK <sup>a</sup>				Sol. SIF (μg/mL)
		mTOR	p4EBP1	P13Kα	CL (L/h/kg)	V <sub>ss</sub> (L/kg)	T <sub>1/2</sub> (h)	F <sup>b</sup> (%)	
<b>2</b>	—	12	162	590 (49X)	1.8	1.14	0.44	24	27
<b>18</b>	—	76	UN <sup>c</sup>	635 (8X)	2.5	1	0.26	ND <sup>d</sup>	1
<b>19a</b>	NH <sub>2</sub>	13	214	763 (58X)	2.3	2	0.85	100	150
<b>20</b>	—	65	507	5840 (89X)	4.1 <sup>e</sup>	1.2	0.25	2 <sup>f</sup>	162
<b>19b</b>	NHMe	63	706	1140 (18X)	4.8	1.3	0.26	29	7
<b>19c</b>	H	141	2170	3020 (21X)	1.9	0.62	0.23	ND	14
<b>19d</b>	NHAc	3	45	47 (13X)	2.6	6.3	0.82	46	200
<b>19e</b>		6	66	122 (21X)	5.8	2.5	0.42	ND	ND
<b>19f</b>		147	6390	1140 (8X)	ND	ND	ND	ND	1
<b>19g</b>		24	276	173 (7X)	ND	ND	ND	ND	ND
<b>19h</b>		35	309	256 (7X)	2.5	3.9	1.59	7 <sup>g</sup>	98
<b>19i</b>		36	146	105 (3X)	6	3.2	0.36	ND	>200
<b>19j</b>		3	85	54 (16X)	6.2	9.1	1.18	ND	175

<sup>a</sup> Rat IV PK, 0.5 mpk, formulation: 100% DMSO.<sup>b</sup> Rat PO PK, 5.0 mpk, formulation: 1%Tween 80, 2%HPMC, 97% H<sub>2</sub>O, pH 2.2 (methanesulfonic acid).<sup>c</sup> UN = Undetermined, failed to achieve proper hill fit to generate IC<sub>50</sub> curve.<sup>d</sup> ND = not determined.<sup>e</sup> Rat IV PK, 0.3 mpk, formulation: 100% DMSO.<sup>f</sup> Rat PO PK, 2.0 mpk.<sup>g</sup> Rat PO PK, 4.0 mpk.

which for **2** and the 6-substituted analogs in Table 2 was around 2 L/h/kg (data not shown) and did not correlate with the low observed in vitro microsomal clearance in rat and human liver microsomes. The compounds demonstrated reasonable permeability and were not substrates for efflux transporters. This lack of in vitro–in vivo PK correlation and our previous experience with related benzimidazole inhibitors **1** suggested that the high in vivo clearance was a result of phase II metabolism.

The results in Table 2 encouraged us to refocus on improving the in vivo PK as a means to increase the exposure of our inhibitors.

In order to understand the mechanism resulting in such high clearance for this series, rat bile duct cannulation studies were performed on parent compound **2**. In this experiment, **2** was administered either PO or IV to male Sprague–Dawley rats and collected urine and bile were analyzed by LCMS–MS to determine the primary metabolites. A small amount of intact parent was excreted in both the IV and PO dosed rats, however, glucuronidation was the primary means of metabolism for **2** for both routes of administration (Fig. 3). The pyrazole was the primary site of glucuronidation, although the triazine amine glucuronide was also detected in sig-



nificant quantities. Minor metabolites were formed through oxidation of the imidazopyridine ring followed by subsequent [O] or [N] glucuronidation.

Several strategies could be employed to address the extensive glucuronidation of **2**, such as eliminating or sterically encumbering the primary site of glucuronidation, or modulating the electronic properties of the molecule to decrease glucuronidation. The free pyrazole NH functionality that was the site of glucuronidation could be capped or replaced by an alternate heteroatom. From previously reported SAR studies, it was clear that the pyrazole affinity pocket group was uniquely effective in providing both potency on mTOR as well as selectivity over structurally related PI3K $\alpha$ .<sup>7</sup> The steep SAR in this highly polar region made addressing this PK liability difficult. Substitution with related heterocycles such as isoxazole provided compounds with significantly diminished potency and selectivity. Methylation of the offending pyrazole NH appeared to be the best path forward, although it led to a marked decrease in potency. In order to mitigate the loss in the potency, the incorporation of the methyl pyrazole was paired with substitution at the 6-position of the imidazopyridine, a change previously shown to boost potency (Table 3). Inhibitor **18** is representative of this SAR change and revealed that although occupation of the ribose pocket with a pyrimidine moiety somewhat mitigated the loss of potency attributed to the methyl pyrazole, the solubility and in vivo PK properties were not improved; furthermore **18** failed to inhibit mTOR activity in the cellular p4EBP1 assay.<sup>18</sup> The high clearance observed for **18** revealed that blocking only one site of glucuronidation was not sufficient to improve the total clearance of these inhibitors.

We speculated that the high in vivo CL of **18** was likely a result of shifting the primary site of glucuronidation from the pyrazole to the triazine. To address this hypothesis, substitution of the hinge-binder moiety to address glucuronidation of the triazine was investigated. It was quickly discovered that the triazine was not particularly amenable to substitution with groups other than alkyl. Attempts to synthesize the triazine amine with acyl or aryl substituents led to chemically unstable compounds. To obviate this problem, a pyrimidine hinge-binder group was investigated with concomitant incorporation of an additional nitrogen in the imidazopyridine ring. This combination of a pyrimidine hinge-binder and an imidazopyridazine core provided **19a**, which was intended to maintain overall structural co-planarity (Table 3). This resulted in a similar potency profile to **2**, but with a greatly increased solubility and bioavailability. Furthermore, the pyrimidine hinge-binder provided a means to

access a variety of substituents, which permitted further exploration of the hinge-binder pocket. Combination of the pyrimidine with the imidazopyridine core was also investigated to test the hypothesis that the two adjacent hydrogens on the attached pyrimidine and imidazopyridine rings would create a steric clash that would lead to a deviation from planarity. Indeed, compound **20** did show diminished potency, but unexpectedly also displayed improved selectivity over PI3K $\alpha$ . This was an interesting discovery; however **20** demonstrated poor bioavailability, cell potency and high in vivo CL.

The results from exploration of the hinge-binder substitution using the imidazopyridazine core are represented by inhibitors **19b–j** (Table 3). The space accessed by these substituents is a narrow cleft that opens up toward solvent (see Fig. 2), and thus only small alkyl or planar groups were tolerated. Acetamide **19d** and pyrazine **19e** were initially designed as substituents that would maintain co-planarity with the pyrimidine hinge-binder. Indeed, groups lacking a heteroatom adjacent to the point of attachment suffered a decrease in potency, potentially due to interaction of the adjacent hydrogens, which could twist the attached ring away from co-planarity (see **19f**). The acetamide **19d**, pyrazine **19e** and pyridazine **19j** gave the best improvement in mTOR cellular p4EBP1 potency, with a slight diminishment of selectivity over PI3K $\alpha$ . The in vivo CL was not improved by these substitutions, but this was anticipated, since the pyrazole affinity pocket group retained its free NH. To understand the potency improvement obtained by these substitutions, both **19d** and **19e** were co-crystallized in the active site of PI3K $\gamma$ . These co-crystal structures (only **19e** pictured, Fig. 4) revealed that both the acetamide and the pyrazine make an additional hydrogen bonding contact with hinge residue VAL882.<sup>19</sup> This contact is best described as a bifurcated H-bonding interaction with the pyrimidine NH and the acetamide CH<sub>3</sub>/pyrazine CH (see Fig. 4).

Taking advantage of the improved potency provided by the incorporation of the acetamide-pyrimidine hinge-binder, this substitution was paired with the methyl pyrazole affinity pocket group in an attempt to circumvent the glucuronidation at both of these sites. The results from this effort on both the imidazopyridazine and imidazopyridine cores are shown in Table 4. For the imidazopyridazine scaffold, capping of both the hinge-binder and the pyrazole led to a decrease in the in vivo CL, but when corrected for free fraction, there was no improvement in the unbound clearance (CL<sub>u</sub>) for the imidazopyridazine scaffold **21b**.<sup>20</sup> The CL<sub>u</sub> for imidazopyridazines **19a** and **21b** were 26.1 and 33.3, respectively, whereas the corresponding CL<sub>u</sub> for imidazopyridines **20** and **21d** were 30.9 and 10.8, respectively. The observed 3-fold improvement in the CL<sub>u</sub> encouraged further exploration of the pyrimidine-imidazopyridine scaffold, which also provided greater selectivity over PI3K $\alpha$ . To improve the potency on mTOR, which was diminished by the incorporation of the methyl pyrazole, substitution of the ribose pocket was explored. Extensive SAR guided by the previous work summarized in Table 3 revealed that 3-pyridyl substituents and 5-membered heterocycles provided the best boost in potency. Methylpyridyl-substituted **21e** demonstrated the best combination of cellular potency on p4EBP1 and selectivity over PI3K $\alpha$ . Of the ribose-substituted analogs, **21e** also demonstrated the best oral exposure, solubility, and in vivo clearance, an overall improvement from our starting point **1**.

The synthesis described in Scheme 1 for imidazopyridine **2** is also representative of the procedures used to synthesize imidazopyridazine scaffold **19**. Palladium-catalyzed coupling of methylchlorotriazine **22**<sup>7</sup> with 2-chloroimidazo[1,2-*a*]pyridine (**23**)<sup>21</sup> provided the imidazopyridine core.<sup>22</sup> Subsequent aminolysis of the remaining triazine chloride with ammonia using microwave irradiation provided triazine-imidazopyridine **24**. The affinity pocket aminopyrazole was installed by Buchwald–Hartwig amination of the chloroimidazopyridine **24** with 3-aminopyrazole catalyzed by

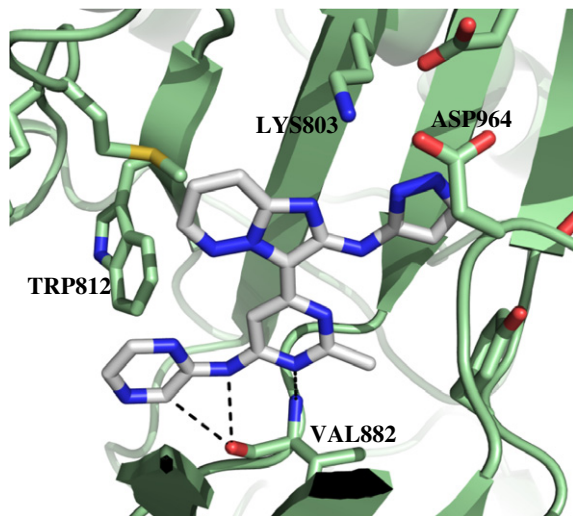
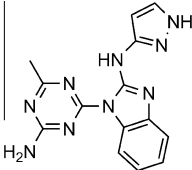
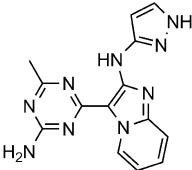
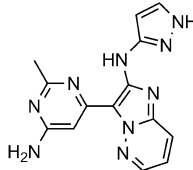
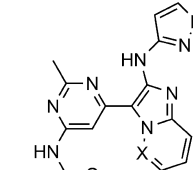
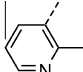
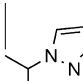
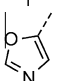
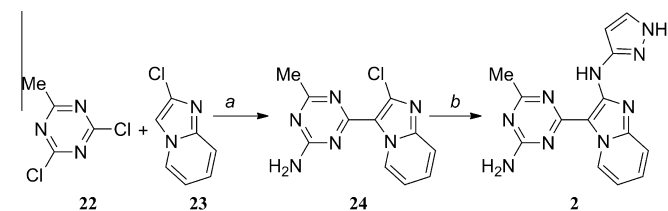


Figure 4. X-ray co-crystal structure of **19e** in PI3K $\gamma$ .

**Table 4**

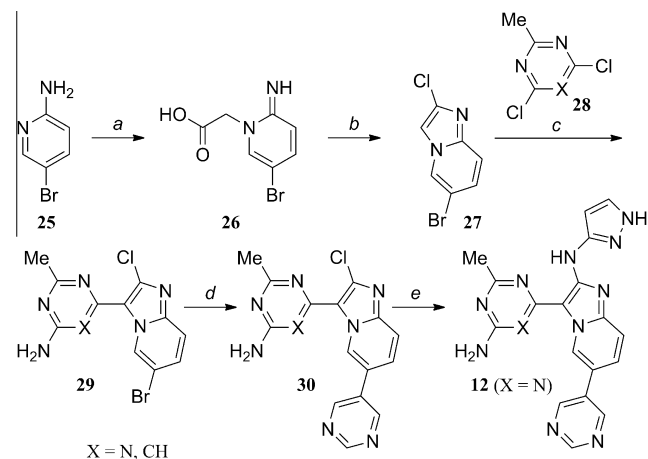
Capping sites of glucuronidation and introducing a ribose substituent improves PK and potency

<div><div></div><div></div><div></div><div></div></div>												
IC <sub>50</sub> (nM)							Rat PK					
Compd	X	R	R <sup>1</sup>	mTOR	p4EBP1	p13Kα	CL <sup>a</sup> (L/h/kg)	AUC (μM h)	V <sub>ss</sub> (L/kg)	T <sub>1/2</sub> (h)	F <sup>b</sup> %	rPPB (%)
<b>1</b>	—	—	—	23	391	798 (35X)	1.9	1.7	1.1	0.72	6	97.2
<b>2</b>	—	—	—	12	162	590 (49X)	1.8	1.8	1.1	0.44	24	97.7
<b>19a</b>	—	—	—	13	210	763 (58X)	2.3	1.0	2.0	0.85	100	91.2
<b>19d (21a)</b>	N	H	H	3	45	47 (13X)	2.6	0.6	2.5	0.82	46	94.4
<b>21b</b>	N	Me	H	55	1230	1660 (30X)	1.1	1.3	0.8	0.39	34	96.7
<b>21c</b>	CH	H	H	9	60	112 (12X)	2.3	0.6	1.2	0.52	ND	ND
<b>21d</b>	CH	Me	H	67	940	4580 (68X)	0.6	2.3	0.6	0.66	4 <sup>c</sup>	94.4
<b>21e</b>	CH	Me		15	230	4290 (286X)	0.6	7.6	1.7	2.8	38 <sup>c</sup>	97.5
<b>21f</b>	CH	Me		16	694	>125,000	0.5	1.8	2.1	4.3	8 <sup>c</sup>	99.6
<b>21g</b>	CH	Me		20	347	3170 (161X)	7.0	0.2	4.1	0.7	3 <sup>c</sup>	ND <sup>d</sup>

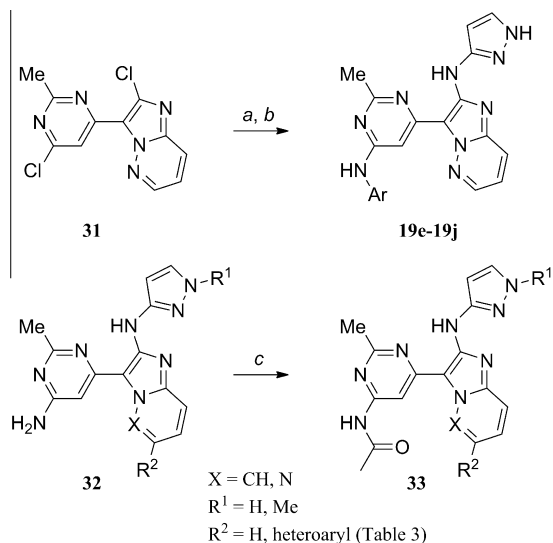
<sup>a</sup> Rat IV PK, 0.5 mpk, formulation: 100% DMSO.<sup>b</sup> Rat PO PK, 5.0 mpk, formulation: 1% Tween 80, 2% HPMC, 97% H<sub>2</sub>O, pH = 2.2 (methanesulfonic acid).<sup>c</sup> Formulation: 30% HPBCD, 70% H<sub>2</sub>O, pH = 2.2 (methanesulfonic acid).<sup>d</sup> ND = not determined.**Scheme 1.** Reagents and conditions: (a) (i) Cs<sub>2</sub>CO<sub>3</sub>, Pd(OAc)<sub>2</sub>, PPh<sub>3</sub>, dioxane, 130–150 °C (μW); (ii) NH<sub>3</sub> (g), (b) 1H-pyrazol-3-amine (or 1-methyl-1H-pyrazol-3-amine), CyPF-*t*-Bu, Pd<sub>2</sub>(dba)<sub>3</sub>, Cs<sub>2</sub>CO<sub>3</sub>, *t*-BuOH/H<sub>2</sub>O (10:1), 100 °C, 50%.

CyPF-*t*-Bu and Pd<sub>2</sub>(dba)<sub>3</sub> in the presence of Cs<sub>2</sub>CO<sub>3</sub> to provide the final product **2** (Scheme 1).<sup>23</sup>

Once it had been established that the 6-position of the imidazopyridine was the most advantageous for substitution with regard to potency improvement, the synthesis was modified to enable rapid diversification of the 6-position (Scheme 2). The most convenient and versatile handle to carry through the synthesis for late-stage analog generation was a bromide, which proved problematic during the initial coupling step between dichloromethyltriazine **22** and 6-bromo-2-chloroimidazo[1,2-*a*]pyridine (**27**). Synthesis of **27** started from 2-amino-5-bromopyridine (**25**). Alkylation of the pyridyl amine with chloroacetic acid provided amino acid **26**. Cyclization, promoted by phosphorylchloride in refluxing acetonitrile, gave the imidazopyridine chloride **27**, which contained the desired bromide functionality for later Suzuki coupling. In order to preserve the bromide functionality, a milder coupling procedure than the one used for the synthesis of **2** had to be employed. Toward this end, deprotonation of the 6-bromo-2-chloroimidazo[1,2-*a*]pyridine

**Scheme 2.** Reagents and conditions: (a) chloroacetic acid, Et<sub>3</sub>N, MeCN, reflux 18 h, 61%; (b) POCl<sub>3</sub>, MeCN, reflux 2 h, 50%; (c) (i) ZnCl(tmp)-LiCl, THF, rt; (ii) 4-chloro-6-methyl-1,3,5-triazin-2-amine, Pd(PPh<sub>3</sub>)<sub>4</sub>, rt; (iii) NH<sub>3</sub> (g) rt, 50–80%; (d) 5-pyrimidinylboronic acid, Na<sub>2</sub>CO<sub>3</sub>, PdCl<sub>2</sub>(dppf)-CH<sub>2</sub>Cl<sub>2</sub>, dioxane/H<sub>2</sub>O, 80 °C, 40–70%; (e) 1H-pyrazol-3-amine, CyPF-*t*-Bu, Pd<sub>2</sub>(dba)<sub>3</sub>, Cs<sub>2</sub>CO<sub>3</sub>, *t*-BuOH/H<sub>2</sub>O (10:1), 100 °C, 39–50%.

**27** using Knochel's LiTMP-ZnCl base,<sup>24</sup> followed by a palladium tetrakis(triphenylphosphine)-catalyzed Negishi cross-coupling with 2,4-dichloro-6-methyl-1,3,5-triazine **28** provided the triazine imidazopyridine core with the bromide intact.<sup>25</sup> This reaction was conveniently telescoped with the amination of the remaining triazine chloride to provide the aminotriazine **29**. A variety of cross-coupling reactions were employed to introduce an assortment of R



**Scheme 3.** Reagents and conditions: (a) Ar-NH<sub>2</sub>, CyPF-*t*-Bu, Pd<sub>2</sub>(dba)<sub>3</sub>, Cs<sub>2</sub>CO<sub>3</sub>, *t*-BuOH/H<sub>2</sub>O (10:1), 90 °C, 18 h, 50–90%; (b) 3-aminopyrazole, CyPF-*t*-Bu, Pd<sub>2</sub>(dba)<sub>3</sub>, Cs<sub>2</sub>CO<sub>3</sub>, *t*-BuOH/H<sub>2</sub>O (10:1), 120 °C, 2 h, 30–50%; (c) (i) Ac<sub>2</sub>O, pyridine, 80 °C, 20–60%; (ii) (only for synthesis of R<sup>1</sup> = H) DCM/MeOH/H<sub>2</sub>O (90/10/1), K<sub>2</sub>CO<sub>3</sub>, rt, 20%.

groups at the 6-position, however, with aryl and heteroaryl groups providing the best potency, Suzuki coupling was used most often, as described for the synthesis of penultimate intermediate **30**. Installation of the affinity-pocket aminopyrazole as previously described in Scheme 1 resulted in final analog **12**. The Knochel coupling procedure described in Scheme 2 was also amenable to the synthesis of **19a**, **20**, and compounds **21a–21f** in Table 4.

Functionalization of the hinge-binder pyrimidine is outlined in Scheme 3. For analogs **19e–19j**, the heteroaryl group attached to the pyrimidine amine was installed using a palladium-catalyzed amination of the dichloride intermediate **31**.<sup>26</sup> Keeping the temperature at 90 °C for this coupling ensured regioselective reaction of the pyrimidine chloride, instead of the imidazopyridine chloride. A second amination was then performed using the identical conditions at 120 °C to couple the affinity pocket pyrazole (Scheme 3, step b). The acetamide functionality could be installed through treatment of the pyrimidine amine **32** with acetic anhydride in pyridine. In the cases where the pyrazole was unsubstituted, a second step was required to cleave the extraneous acetate from the pyrazole to provide inhibitors **19d** and **21b**.

Starting from the previously reported triazine-benzimidazole **1**, which had less desirable PK properties, modifications were made to the central benzimidazole ring to improve solubility. This effort resulted in triazine-imidazopyridine **2**, which demonstrated improved solubility and bioavailability when compared to **1**. This improvement was sufficient to allow the testing of **2** in multiple in vivo studies demonstrating up to 84% TGI at a 60 mpk oral dose. While this outcome was encouraging, the triazine-imidazopyridine series still suffered from high in vivo clearance that was not predicted by in vitro liver microsome experiments. Rat BDC metabolism studies indicated that glucuronidation was the primary means of metabolism and was likely the case for the high observed in vivo clearance. Subsequent efforts focused on further modifications to the scaffold to block the sites of glucuronidation while maintaining potency and selectivity. This resulted in pyrimidine-imidazopyridine **21e**, which demonstrated improved in vivo clearance and selectivity over both **1** and **2**, while maintaining sufficient cellular potency on mTOR substrate p4EBP1.

## Acknowledgments

The authors would like to acknowledge Wei Hu, Tisha San Miguel, and Leeanne Zalameda for enzyme and cell assay support. We are also grateful to Loren Berry, Xuhai Be, Liyue Huang, Meghan Langley, and Jonothan Roberts for PKDM support. Thanks to Pete Yakowec and Jin Tang for PI3Kγ expression and purification as well as Huilin Zhao and Linda Epstein for mTOR expression and purification.

## References and notes

- Zoncu, R.; Efeyan, A.; Sabatini, D. M. *Nature Rev.* **2011**, *12*, 21.
- (a) Rini, B. I. *Clin. Cancer Res.* **2008**, *14*, 1286; (b) Rini, B.; Kar, S.; Kirkpatrick, P. *Nat. Rev. Drug Disc.* **2007**, *6*, 599.
- Motzer, R. J.; Escudier, B.; Oudard, S.; Hutson, T. E.; Porta, C.; Bracarda, S.; Grünwald, V.; Thompson, J. A.; Figlin, R. A.; Hollaender, N.; Kay, A.; Ravaud, A. *Cancer* **2010**, *116*, 4256.
- Carracedo, A.; Pandolfi, P. P. *Oncogene* **2008**, *27*, 5527.
- Luo, J.; Sobkiw, C. L.; Hirshman, M. F.; Logsdon, M. N.; Li, T. Q.; Goodyear, L. J.; Cantley, L. C. *Cell Metab.* **2006**, *3*, 355.
- (a) Schenone, S.; Brullo, C.; Musumeci, F.; Radi, M.; Botta, M. *Curr. Med. Chem.* **2011**, *18*, 2995–3014; (b) Garcia-Echeverria, C. *Bioorg. Med. Chem. Lett.* **2010**, *20*, 4308.
- Peterson, E. A.; Andrews, P. S.; Be, X.; Boezio, A. A.; Bush, T. L.; Cheng, A. C.; Coats, J. R.; Colletti, A. E.; Copeland, K. W.; DuPont, M.; Graceffa, R.; Grubinska, B.; Harmange, J.-C.; Kim, J. L.; Mullady, E. L.; Olivieri, P.; Schenkel, L. B.; Stanton, M. K.; Teffera, Y.; Whittington, D. A.; Cai, T.; La, D. S. *Bioorg. Med. Chem. Lett.* **2011**, *21*, 2064.
- (a) Li, Q.; Chu, D. T. W.; Claiborne, A.; Cooper, C. S.; Lee, C. M.; Raye, K.; Berst, K. B.; Donner, P.; Wang, W.; Hasvold, L.; Fung, A.; Ma, Z.; Tufano, M.; Flamm, R.; Shen, L. L.; Baranowski, J.; Nilius, A.; Alder, J.; Meulbroek, J.; Marsh, K.; Crowell, D.; Hui, Y.; Seif, L.; Melcher, L. M.; Henry, R.; Spanton, S.; Faghih, R.; Klein, L. L.; Tanaka, S. K.; Plattner, J. J. *J. Med. Chem.* **1996**, *39*, 3070; (b) Ishikawa, M.; Hashimoto, Y. *J. Med. Chem.* **2011**, *54*, 1539; (c) Gleeson, M. P. *J. Med. Chem.* **2008**, *51*, 817.
- Ambit, kinome scan binding assay measured at 1 μM, <http://www.kinomescan.com/>, last accessed 5–14-2012.
- In our previous report,<sup>7</sup> **1** was dosed IP due to solubility constraints.
- S6 instead of p4EBP1 was measured to determine the inhibition of mTORC1 due to the lack of a suitable antibody for p4EBP1 in mouse.
- pAKT levels in the liver lysate were measured using an MSD assay method. Measurement of pAKT inhibition in HGF-stimulated liver is a common practice within the mTOR field, see: Feldman, M. E.; Apsel, B.; Uotila, A.; Loewith, R.; Knight, Z. A.; Ruggero, D.; Shokat, K. M. *PLoS Biol.* **2009**, *7*, 1.
- X-ray coordinates deposited in the Cambridge Crystallographic Data Centre, PDB code 4FHH.
- PI3Kγ shares significant homology with the mTOR active site and is commonly used to understand the binding trajectory of mTOR inhibitors in the ATP active site.
- The narrow cleft adjacent to the hinge binder in mTOR is caused by TRP779, which overlays with PI3Kγ and α at the VAL881 residue.
- We considered the p4EBP1 cellular assay to be the most important measure of mTOR potency, since it determined activity on mTOR signaling in the presence of all the associated proteins that constitute the mTOR complex, whereas the kinase assay consisted of only the mTOR kinase.
- UN = Undefined: failed to achieve a hill fit in the assay, in this case, no significant inhibition was observed.
- X-ray coordinates deposited in the Cambridge Crystallographic Data Centre, PDB code 4FHK.
- (a) Smith, D. A.; Di, L.; Kerns, E. H. *Nat. Rev. Drug Disc.* **2010**, *9*, 929; (b) Pellegatti, M.; Pagliaruso, S.; Solazzo, L.; Colato, D. *Expert Opin. Drug Metab. Toxicol.* **2011**, *9*, 1009.
- Maxwell, B. D.; Boye, O. G.; Ohta, K. J. *Label. Comp. Radiopharm.* **2005**, *48*, 397.
- Koubachi, J.; Kazzouli, S. E.; Berteina-Raboin, S.; Mouaddib, A.; Guillaumet, G. *Synlett* **2006**, 3237.
- For full experimental procedures, please see: Bode, C.; Boezio, A.; Cheng, A. C.; Choquette, D.; Coats, J. R.; Copeland, K. W.; Huang, H.; La, D.; Lewis, R. et al. *PCT Int. Appl.* **2010**, WO 2010132598.
- Mosrin, M.; Knochel, P. *Org. Lett.* **1937**, 2009, 11.
- This procedure was also used to prepare pyrimidine imidazopyridine **20** and related compounds.
- This dichloride intermediate could be synthesized using the direct coupling conditions outlined in Scheme 1, step a, or using the Knochel coupling described in Scheme 2.